Int. J. Heat Mass Transfer. Vol. 16, pp. 2305–2319. Pergamon Press 1973. Printed in Great Britain

DIRECT CONTACT HEAT TRANSFER WITH CHANGE OF PHASE: CONDENSATION OF A BUBBLE TRAIN

D. MOALEM, S. SIDEMAN, A. ORELL and G. HETSRONI
Technion—Israel Institute of Technology, Haifa, Israel

(*Received* 28 *June* 1972 *and in revised form* 1 *May*, 1973)

Abstract—Solution of the coupled velocity and temperature fields associated with the condensation of a single or two-phase bubble train is used to obtain the bubbles' radii as a function of time (or height), frequency, temperature driving force and inerts concentration.

The reliability of the solution procedure is demonstrated by its convergence at zero frequency to other solutions of single bubble condensation and by the good agreement of the calculated results with experimental data.

NOMENCLATURE

A, matrix;
A, constant;
a, constant;
$\bar{a}$, constant;
B, constant;
$\boldsymbol{B}$, radial distance vector;
b, constant;
$\bar{b}$, constant;
c, constant;
$\bar{c}$, constant;
D, center to center distances between bubbles;
$\bar{d}$, constant;
F_w, wake velocity factor;
F, bubble frequency;
F_0, Fourier modules $(\alpha t/R_0^2)$;
$\boldsymbol{I}$, intensity vector;
Ja, Jacob no. $[\rho_l Cp_l (T^* - T_\infty)/(\rho_v \lambda)]$;
K, distance between edge of line element and point in field;
k_v, velocity factor;
L, length of line element;
m, index of reference element;
N, number of bubbles in a train;
n, number of line elements;
P, body point;
Pe_0, Péclét number $(= 2R_0 U_\infty^F/\alpha)$;
Pe, Péclét number $(= DU_\infty^F/\alpha)$;
Q, point outside bubbles envelope;
r, radial coordinate;
R, radius of bubble;
r_w, radius of contact area of wake and tailing bubble;
T, temperature;
T_∞, approach temperature;
T^*, saturation temperature, corrected for hydrostatic pressure;
t, time;
t_c, time to final condensation;
U_∞, velocity of rise of single bubble in an unbounded media;
U_∞^F, frequency-dependent velocity of rise;
v_r, radial velocity component;
v_z, axial velocity component;
X, dimensionless axial coordinate (z/D);
Y, dimensionless coordinate $(= r/D)$;
z, axial coordinate.

Greek letters

α, thermal diffusivity, continuous phase;
β, dimensionless bubble radius (R/R_0);
β_f, dimensionless bubble radius (R_f/R_0);
γ, angular coordinate;
θ, dimensional temperature $(= (T - T_\infty)/(T^* - T_\infty))$;

ρ, density;
η, intensity of line element;
ϕ, potential function;
Φ, dimensionless potential function, equations (20)–(21);
ψ, stream function;
Ψ, dimensionless stream function, equations (20)–(21);
Ψ_t, transformed dimensionless stream function;
ξ, constant;
ζ, constant;
τ, $Ja\, Pe_\delta^{\frac{1}{2}}\, F_0$.

Subscripts

0, lower bound (for frequency); initial (radius);
1, leading bubble;
2, tailing bubble;
∞, infinity (approach or radial);
c, complete contact (angle);
f, final;
i, index, no. of element; number of bubble;
j, index, body point;
l, liquid, continuous phase;
L, condensed bubble, liquid;
M, a point in flow field;
m, mth line element;
mp, relation between element m and body point p;
n, number of elements, total;
p, body point;
r, radial;
s, separation (angle);
v, uncondensed bubble; vapor;
w, wake; wall;
z, axial.

Superscripts

F, frequency dependence;
0, edge of line element at $L = 0$;
L, edge of line element at $L = L$.

1. INTRODUCTION

BUBBLE trains, in which the bubbles diminish in size while in motion through a liquid, are encountered in numerous engineering applications involving heat and mass transfer. Of particular interest is the study of bubble condensation in two and three phase systems, associated with the design of efficient exchangers capable of heat recovery with small temperature driving forces. These direct contact heat exchangers provide the advantages of smaller flow rates of the transfer fluid, convenient separation of the fluids, and very high heat-transfer coefficients. This mode of operation is applicable to any pair of fluid systems, provided a suitable immiscible transfer fluid is chosen.

Unlike condensation in a single-component system (say, steam in water), where the condensing vapor merges with the surrounding continuous liquid, the condensed vapor in these immiscible systems (say, pentane or Freon in water) remains within the confines of the bubble wall. This sytem thus consists of the vapor and two liquid phases. For ease of reference and in order to avoid confusion when non-condensables are present in the vapor, we denote these bubbles in the two-fluid system as "two-phase bubbles". By analogy, the bubble in a single-component system is denoted as a "single-phase bubble".

Practically all past studies relate to bubble growth and collapse of a single bubble and with only a few exceptions these studies are limited to the radial motion of a stagnant bubble.

The first exact numerical solution for bubble collapse in a single-component system, including the effects of the translatory motion of the bubble, is due to Wittke and Chao [1]. Following an earlier experimental study [2] a general numerical solution for a "two-phase bubble" was presented by Isenberg and Sideman [3]. For a "single-phase" bubble this solution degenerates to the previous solution [1]. An approximate analytical quasi-steady state solution for the condensation of single and two-phase bubbles, including the effects of con-

centration distribution of the non-condensables within the bubble, was recently presented [4, 5]. The calculated results are in good agreement with the experimental work of Isenberg [3] and Moalem [4].

The present study deals with a train of bubbles continuously originating at the same source. Based on a simplified energy balance, an approximate solution for the collapse rate of a bubble in a bubble train was recently presented [6]. The solution was obtained by treating one bubble as representing the bubbles in the train, and calculating the collapse rate for the frequency-dependent rise velocity and the temperature driving force along the bubble's path.

While the flow field around a single unbounded bubble can be solved independent of the temperature field, the bubble train is a continuous, infinite process, and requires a simultaneous solution of the temperature and flow fields. An iterative procedure is thus required: a bubble train is assumed and the flow field is solved. The ensuing solution of the energy equation leads, through the collapse rate, to a new configuration of the bubble train.

The first part of this work is therefore devoted to the solution of the flow field around a specific bubble train of decreasing radii (Fig. 1). The uncondensed bubble is at the bottom of the column while the smallest bubble, at a finite final condensation stage, is leaving the top. Bubbles at intermediate condensation stages are equally spaced in between these two positions. Hick [7] and Basset [8] presented a solution for potential flow around two identical solid spheres and Michael [9] solved for the flow around a row of identical spheres. Herman [10] and, more recently, Isenberg and Sideman [11] presented solutions for potential flow around two vertically adjacent bubbles of different radii, including radial motion of the interface. Extensions of solutions of the ensuing Newmann problem by the method of successive approximations (negating harmonics on the incompatible boundary conditions) to a multi-bubble column is quite tedious and complicated.

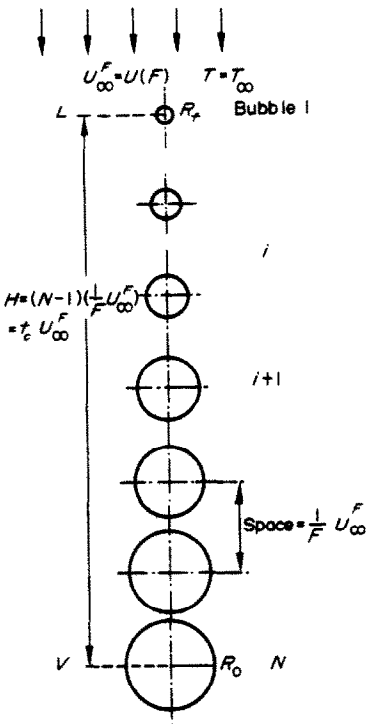

FIG. 1. Schematic presentation of a bubble train.

A new technique was utilized here which is both faster and allows mapping of the whole flow field.

2. THE FLOW FIELD

2.1 *The bubble train*

For a given bubble frequency F and given temperature of the surrounding liquid, the bubble train (Fig. 1) is defined, subject to the following simplifications: (a) The instance of any bubble detachment from the origin is taken as zero-time. (b) The column consists of all the bubbles present at time-zero, including the highest bubble at its final condensation stage. (c) The system is at periodic steady state, i.e. it repeats itself at time intervals of $1/F$. (d) All incoming bubbles move through the same path

and reach the identical final condensation stage (complete or partial condensation, depending on the concentration of non-condensables).

2.2 *Method of solution*

For the purpose of the analysis, the bubble train is assumed to be stationary while the fluid flows around it. This is permissible in view of the simplifying assumption that the solution is applicable to a periodic steady state. In other words, the system is frozen at zero-time and solved as a stationary system.

The potential flow model, adequately established for flow around single gas bubbles [11], is extended to the flow configuration at hand. This is consistent with the recent study of Ishii and Johnson [12] on flow in bubble swarms. Thus, the solution is based on finding the proper combination of hydrodynamic doublets (sources, sinks) and dipoles which, combined with the linear approach velocity U_∞^F yields the velocity field in terms of the potential and stream functions around the axially symmetrical bubble.

It can readily be shown that the stream and potential functions for a line element i, of length L, located on the axis of symmetry z, are given by [13]:

$$\psi_i = \frac{\eta_i}{4\pi}[K_{ir}^0 - K_{ir}^L] \tag{1}$$

and

$$\phi_i = \frac{\eta_i}{4\pi}\ln\frac{K_{ir}^L(1-\cos\gamma^L)}{K_{ir}^0(1-\cos\gamma^0)} \tag{2}$$

where η_i denotes the intensity of the element per unit length. K_{ir}^0 and K_{ir}^L are the distances from points $z = 0$ and $z = L$ on the element i, at angles γ^0 and γ^L, respectively, to a point located at a radial distance r from the z coordinate (Fig. 2).

The contribution of an unperturbed uniform flow field U_∞^F to the stream function at this point is given by

$$\psi_{U_\infty^F} = -\tfrac{1}{2}U_\infty^F r^2. \tag{3}$$

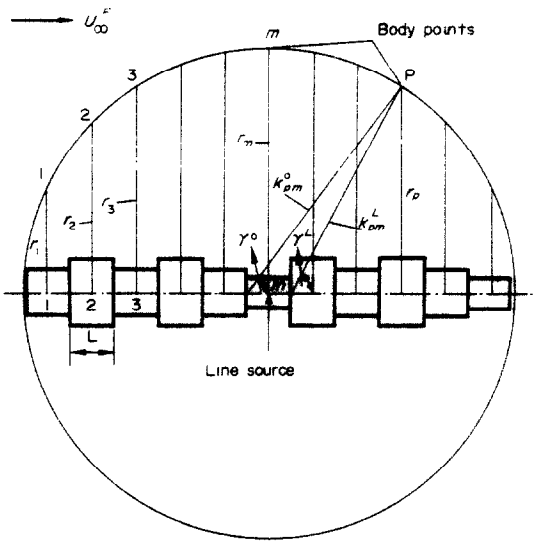

FIG. 2. Construction of streamlines from hydrodynamic line sources.

The shape of the column is determined by the distance between the hydrodynamic elements and their intensities under the constraints that the sum of the intensities is zero and that the sum of the overall stream function is nullified on the interfaces.

Consider a succession of n line elements, each of length L_i but of different intensity, touching each other head to tail on the z coordinate. The stream function at "body point" P on the interface, is obtained by summing the contributions due to all n elements and the uniform flow field. Hence,

$$\psi_P = \sum_{i=1}^{n}\frac{\eta_i}{4\pi}[K_{ip}^0 - K_{ip}^L] - \tfrac{1}{2}U^F r_p^2 \equiv 0 \tag{4}$$

where r_p is the radial distance from the line of symmetry to point P. Thus, for n elements and n interfacial body points we obtain the following n by n matrix:

$$\boldsymbol{AI} = \boldsymbol{B} \tag{5}$$

where

$$A = [A_{ij}] = (K^L_{ij} - K^L_{ij}]\ \frac{1}{4\pi};\ i,j = 1,2,\ldots n$$

$$I = \begin{pmatrix} \eta_1 \\ \cdot \\ \cdot \\ \cdot \\ \eta_n \end{pmatrix} \qquad B = \tfrac{1}{2}\, U^F_\infty \begin{pmatrix} r_1^2 \\ \cdot \\ \cdot \\ \cdot \\ r_n^2 \end{pmatrix}. \qquad (6)$$

The solution of the matrix under the constraint $\sum_{i=1}^{n} \eta_i L_i = 0$ yields the intensity vector I which is consequently used to calculate the stream and potential functions at any point Q in the field. These are given by:

$$\psi_Q = \sum_{i=1}^{n} \frac{\eta_i}{4\pi} [K^0_{iQ} - K^L_{iQ}] - \tfrac{1}{2}\, U^F_\infty\, r_Q^2 \quad (7)$$

$$\phi_Q = \sum_{i=1}^{n} \frac{\eta_i}{4\pi} \ln \frac{K^L_{iQ}(1 - \cos\gamma^L)}{K^0_{iQ}(1 - \cos\gamma^0)} - U^F_\infty z \quad (8)$$

where r_Q is the radial distance from the line of symmetry (z axis) to point Q, K^L_{iQ} and K^L_{iQ} are the respective distances between the two edges of line element i and point Q, and $-U^F_\infty z$ is the contribution of the unperturbed uniform flow field to the potential function.

2.3 *The governing parameters*

Solution of equations (7) and (8) requires the knowledge of the following interrelated parameters.

The approach velocity. Single bubble studies [14] show that the velocity of rise of bubbles, 0·2–0·8 cm dia, is independent of their diameter. Assuming that the same holds true for bubbles in a train, the velocity of rise of the bubbles in the column is taken to depend only on the interaction between successive bubbles, hence on the frequency of bubble production, but to be constant at each frequency.

With reference to Fig. 3, the frequency dependent rise velocity of a chain of bubbles,

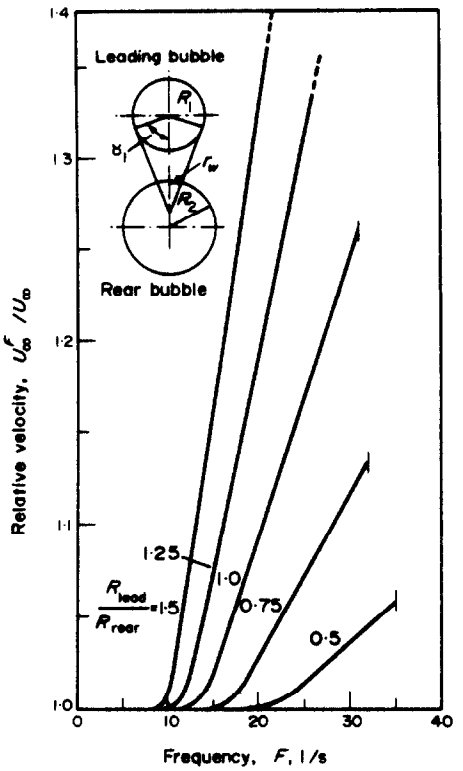

FIG. 3. Effect of frequency on rise velocity.

or the approach velocity, is given by [6, 13]:

$$\left(\frac{U^F_\infty}{U_\infty}\right)^2 = \frac{R_2^2}{R_2^2 - r_w^2(1 - F_w^2)} \qquad (9)$$

where r_w is the radius of the projected contact area between the wake and the rear bubble of radius R_2 ($= R_N$); F_w is the fraction of velocity decrease in the wake region, given by [15]:

$$F_w = \frac{U^F_\infty - U_w}{U^F_\infty} \simeq 0{\cdot}1 \qquad (10)$$

where U_w is the forward velocity in the wake, corrected for internal circulation within the wake. The numerical value for U_∞, the free rise velocity of a single bubble, is taken as that corresponding to the lowest bubble in the column, R_0, consistent with earlier studies [3, 4] indicating that bubble collapse does not

affect the rise velocity. It is noted, however, that at large temperature driving forces, hence higher collapse rates, the free rise velocity of the larger bubbles in the earliest condensation stages is not quite constant. Also, the free rise velocity is not constant for condensation in viscous media, such as pentane in aqueous glycerine solutions.

It is noteworthy that the bubbles in an ascending chain are not accelerating with respect to a fixed coordinate system. Unlike the pairs of bubbles in which the rear bubble accelerates, collides and coalesces with the leading bubble [16], no coalescence was noted with pentane bubble trains condensing in pentane, distilled water or aqueous glycerine solutions.

The distance between the centers. The relationship between the frequency and the distance between the bubbles is particularly useful since it is directly associated with the final condensation time t_c. For a constant U_∞^F, calculated by equation (9), the distance between two consecutive bubbles is given by:

$$D = \frac{1}{F} U_\infty^F \tag{11}$$

while the distance between the "initial" and "final" bubbles, of radius R_0 and R_f respectively, in a bubble train containing N bubbles, is given by:

$$\sum_i^N D_i = (N-1)\frac{1}{F} U_\infty^F = t_c U_\infty^F \tag{12}$$

or

$$t_c = (N-1)/F. \tag{13}$$

The contact and separation angles. It is reasonable to expect that the contact and separation angles depend upon the distance between the bubbles. For truly potential flow, these angles are 0 and π, respectively, independent of the distance. For viscous systems, the separation angle γ_s can be determined, at least approximately, by the well-known Reynolds number dependent correlations for flow around solid spheres [17]. The approach angle γ_c is determined with reference to the wake of the preceding bubble and the distance between the bubbles. Between these two angles, the enveloping stream function $\psi = 0$ coincides with the walls of the bubble. Since the angles vary with each system, they are determined separately and treated as input data.

The radii of the bubbles in the column, R_i, are assumed for the first iteration, while for the next iterations the radii resulting from the previous iteration are used.

2.4 *The calculated flow field*

The system of equations (5)–(8) was solved by utilizing Gause elimination technique. The input data consisted of R_0, F, U_∞ (hence U_∞^F), γ_c, γ_s, n, L and R_f. The number and length of the line elements varied with R_i, depending on the length of the envelope ($\Psi = 0$) between γ_c and γ_s of each bubble. Double precision techniques were employed, utilizing a PL/1 compiler. The program was checked by computing the limiting case of a single bubble and comparing with the analytical solutions, whereby:

$$\phi = U_\infty R \left[1 + \frac{1}{2}\left(\frac{R}{r}\right)^3\right] \cos\gamma \tag{14}$$

$$\psi = U_\infty R^2 \left[1 - \left(\frac{R}{r}\right)^3\right] \sin^2\gamma. \tag{15}$$

Figure 4 represents the calculated axially symmetrical flow fields around a given bubble train.

Whereas non-dimensionalizing equations (14) and (15) yields a ψ–ϕ network invariant in R, the ψ–ϕ net of equations (7) and (8) for the bubble train varies with R_i as well as with D. Thus, a new network must be computed for each change in R_i or D. Furthermore, the inverse transformation from ψ–ϕ to r–z in the single bubble case is relatively simple (elimination of γ from equations (14) and (15) yields a 9th order equation in r which is routinely solved [18]). However, the comparable transformation to r–z from the ϕ–ψ plane utilizing equations

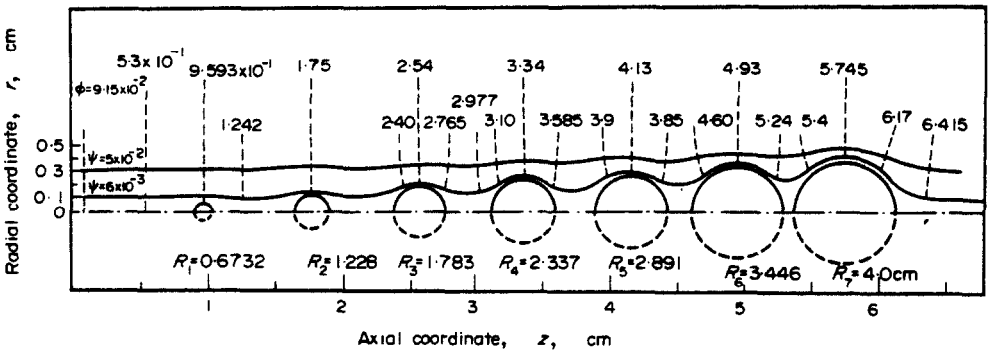

FIG. 4. Calculated potential and streamlines of a given bubble train.

(7) and (8) is quite cumbersome, since there is no way to eliminate one of the unknowns. Moreover, values of ϕ–ψ and their derivatives are needed for each of the iterations (see below) required in the solution of the energy equation. A special interpolation program, utilizing the Newton–Raphson procedure and the Fibbonachi search technique was used to map the ϕ–ψ plane, and an iterative procedure to remap the r–z plane was adopted [13].

3. THE TEMPERATURE FIELD

3.1 *General*

The solution of the temperature field requires that a bubble train under given conditions be assumed, calculating the flow and temperature fields and, consequently, the heat fluxes and the corresponding collapse rates. A new train is then calculated and the iterative procedure is continued until the bubble train corresponds to that calculated by means of the heat fluxes. The results can then be presented as plots of bubble radii versus time (or height), with the frequencies and temperature driving forces as parameters.

3.2 *The mathematical formulation*

The steady state energy equation, in cylindrical coordinates, for an axially symmetrical case, is given by

$$v_r \frac{\partial T}{\partial r} + v_z \frac{\partial T}{\partial z} = \alpha \left[\frac{1}{r} \frac{\partial}{\partial r} \left(r \frac{\partial T}{\partial r} \right) + \frac{\partial^2 T}{\partial z^2} \right]. \quad (16)$$

The solution of equation (16) requires the explicit knowledge of the velocity components. These may be taken from the solution for the potential flow field. However, no solution is available at present for the comparable viscous flow, which is encountered in the condensation of two-phase bubbles. Following earlier single bubble studies [3, 4], we introduce here the velocity factor

$$k_v = 0{\cdot}25\, Pr^{-\frac{1}{3}} \quad (17)$$

designed to modify the convective terms so that the resulting solution of the energy equation would correspond to the actual viscous convective terms. Note that $k_v = 1$ for truly potential flow. The intrinsic merit of this approach is that it allows for a general solution of the energy equation for both potential and modified-potential flows, and circumvents the need for explicit velocity terms in the viscous flow field.

Utilizing the center-to-center distance between the bubbles, D, as the characteristic length, we define:

$$Y = r/D; \quad X = z/D; \quad J = j/U_\infty^{F2}$$
$$\Phi = \phi/U_\infty^F D; \quad \Psi = \psi/U_\infty^F D^2;$$
$$Pe = U_\infty^F D/\alpha; \quad A = JY^2; \quad (18)$$
$$B = 2v_z/U_\infty^F; \quad C = J\, Pe\, k_v$$

where

$$j = \left(\frac{\partial \phi}{\partial r} \right)^2 + \left(\frac{\partial \phi}{\partial z} \right)^2 = v_r^2 + v_z^2. \quad (19)$$

For large Péclét numbers (> 1000), the tangential conduction, in the ϕ direction, is negligible compared with the convective term. To obtain better accuracy near the bubble, and reduce calculations away from it, we introduce a step transformation:

$$\Psi = \begin{cases} -\Psi_t & \text{for } 0 \leqslant \Psi_t \leqslant \Psi_{tI} \\ -\Psi_{tI} - \xi(\Psi_t - \Psi_{tI})^{\zeta} & \text{for } \Psi_t > \Psi_{tI} \end{cases} \quad (20)$$

where Ψ_{tI} is the value of Ψ_t at the end of the linear zone and ξ and ζ are arbitrarily chosen values. Equation (16) becomes:

$$A_t \frac{\partial^2 \theta}{\partial \Psi_t^2} + B_t \frac{\partial \theta}{\partial \Psi_t} + C \frac{\partial \theta}{\partial \Phi} = 0 \quad (21)$$

where

$$\theta = \frac{T - T_\infty}{T^* - T_\infty}; \qquad A_t = A\left(\frac{\partial \Psi_t}{\partial \Psi}\right);$$

$$B_t = B\frac{\partial \Psi_t}{\partial \Psi} + A_t\left(\frac{1-\xi}{\Psi_t - \Psi_{tI}}\right). \quad (22)$$

It is assumed that the heat transfer between the bubbles and the continuous phase is essentially done across the enveloping stream line $\psi = 0$, coinciding with the wall of bubbles. Thus;

$$\begin{aligned} &\Phi = \Phi_0, && \theta = 0 \\ &\Psi = \infty, && \partial\theta/\partial\Psi = 0 \\ &\Psi = 0, && \theta_0 = 1 \text{ on the interface} \\ & && \theta_0 = 0 \text{ between bubbles} \end{aligned} \quad (23)$$

where Φ_0 is the upper limit of the Φ-field, and θ_0 is the value of θ on the inner stream line $\Psi = 0$. At very high frequencies, as $D \simeq 2R_i$, it may be physically meaningful to assume that the space between the bubbles in the column contains fluid which is essentially at the saturation temperature, i.e. $\theta = 1$ on $\Psi = 0$.

The outline of the solution for the temperature field and the local gradients is presented in Appendix A.

3.3 *The collapse rate*

The heat balance at the interface along the line $\Psi = 0$:

$$4\Pi R^2 \rho_{v,w} \lambda \frac{dR}{dt} = \int_{\gamma_c}^{\gamma_s} 2\Pi k \left.\frac{dT}{dn}\right|_{r=R} (R \sin\gamma)(R\, d\gamma) \quad (24)$$

yields the collapse rate for each bubble:

$$\dot{R} = \frac{k}{2\rho_{v,w}\lambda} \int_{\gamma_c}^{\gamma_s} \left.\frac{dT}{dn}\right|_{r=R} \sin\gamma\, d\gamma \quad (25)$$

where $\rho_{v,w}$ is the vapor density near the interface.

The new radii of the bubbles in the train is now computed by averaging the collapse rate of bubble i moving at the time interval $1/F$ to the $i-1$ position (Fig. 1) i.e.:

$$R_{i-1}^{\text{new}} = R_i^{\text{old}} - \frac{1}{F}\frac{(R_i + R_{i-1})}{2}. \quad (26)$$

The values thus obtained are then used again as the initial radii for the next iteration and the process is continued until the collapse rate corresponds to the decrease in bubble size in the train.

An outline of the general iteration procedure is given in Appendix B.

3.4 *Effect of non-condensables*

In deriving equations (23) and on, it has been assumed that the system consists of pure vapor, and condensation proceeds at T^*, the vapor saturation temperature, corresponding to the system pressure. However, inert non-condensables (usually air) are present in practically all systems. These reduce the partial pressure of the condensing vapors and decreasc the corresponding saturation temperature. As collapse proceeds, the effect of these inerts increases until condensation is halted, as $T_w \to T_\infty$, where T_w denotes the internal wall temperature.

The effect of non-condensables in bubble condensation has been extensively treated elsewhere [3–5]. It suffices to note that in this case

T_w replaced T in equation (22) [and $\theta_0 = \theta_w \neq 1$, equation (23)] and affects the ensuing calculations based on it. For the simplest case of homogeneous distribution of the inerts inside the bubbles, the value of θ_w is given by [3, 4]:

$$\theta_w = \frac{T_w - T_\infty}{T^* - T_\infty} = \frac{\beta^3 - \beta_f^3}{\beta^3 - 1/G} \tag{27}$$

where the term $1/G = \rho_v/\rho_L$, due to the condensed fluid which accumulates inside the two-phase bubble, vanishes for a single-phase bubble. $\beta = R/R_0$ and β_f is the radii ratio of the final and initial bubbles in the column. In the absence of inerts $\beta_f = 0$ for the single phase bubble and $\beta_f = G^{-\frac{1}{3}}$ for the two-phase bubble. For a given initial concentration of inerts in the incoming vapor, Γ (mole fraction):

$$\beta_f = \left| \frac{\hat{R} T^{*2} \Gamma}{\lambda (T^* - T_\infty)} + \frac{1}{G} \right|^{\frac{1}{3}} \tag{28}$$

where $\hat{R}$ is the specific gas constant. Again $1/G$ vanishes for a single-phase bubble. Somewhat different expressions for β_f and T_w are obtained when a concentration gradient within the bubble is considered [5]. Note that in some cases it may be more convenient to obtain β_f, rather than Γ, experimentally.

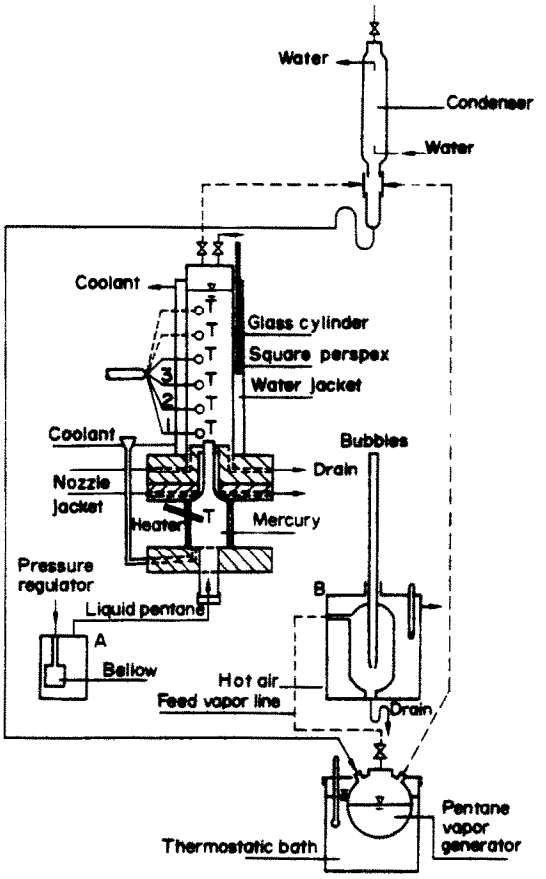

FIG. 5. Condensation test cell.

4. EXPERIMENTAL

The experimental setup shown schematically in Fig. 5, is a modification of the one used previously for single bubble studies [4, 5, 13] and only the essential features are outlined here.

The apparatus included: (1) a condensation cell—a glass column surrounded by a square water-jacket, (2) bubble injection mechanisms, at the bottom, and (3) a movie camera.

The continuous phase in the condensation column was either pentane or distilled water. Water was circulated in the square water jacket, in order to maintain the temperature of the column. This jacket also eliminated visual distortion of the bubbles.

The pentane bubbles were injected into the bottom of the column through a capillary (B) passing a 7-cm layer of relatively hot mercury. (In some runs, liquid drops were injected at the bottom of the mercury layer.) The frequency of the bubbles was varied by means of pressure bellows, actuated by external pressure, and by using various capillaries. All the relevant temperatures were measured and recorded with an estimated error of $\pm 0{\cdot}05°C$.

The bubbles were photographed with a cine-camera at a speed of 64 fps. With the relatively large bubbles and low ΔT^* used here, the 64 fps camera yielded some 20–30 data points per run. The collapse rates were obtained by a frame to frame analysis. The time-scale error is within $\frac{1}{64}$ sec and the bubble dimensions within 2 per cent.

5. RESULTS AND DISCUSSION

In order to establish the reliability of the outlined approach, the solution procedure was checked by solving for the condensation rate of a single bubble. Note that in this case the flow field program remains unchanged while the energy equation (equation 16) must be modified to include the unsteady state term (which does not appear in the periodic steady-state solution assumed for the continuous bubble train). As seen in Fig. 6 the results obtained here are in

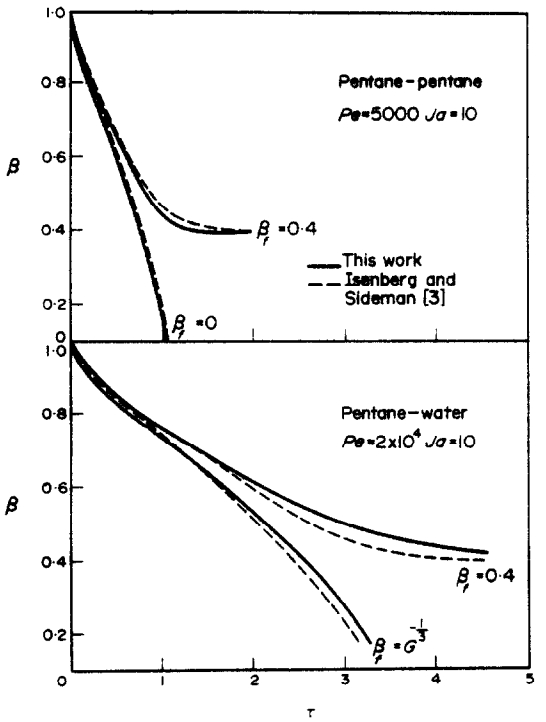

FIG. 6. Convergence test for single bubbles.

excellent agreement with those reported by Isenberg and Sideman [3] for a single pentane bubble condensing in either pentane or water.

The effects of the initial bubble size, type of of system and inerts content are essentially similar to those encountered in the earlier single bubble-condensation studies [3, 4]. We shall therefore concentrate mainly on the effects of frequency on the condensation rate of a bubble train.

A comparison between the results obtained here and the approximate "analytical" solution [6] for condensation of various bubble trains at different operating conditions is presented in Figs. 7 and 8. Also included in Figs. 7 and 8 is the curve for a single collapsing bubble at the same temperature driving force. Real time was used in the abcissa in order to render a better physical feeling.

As seen from these figures—and others not presented here—the agreement between the two solutions is very good, particularly at frequencies above 10 bubbles per s. This is understandable in view of the simplified energy balance used in the analytical solution whereby all the heat released during the condensation accumulates in the space between the consecutive bubbles. Evidently, this assumption is fairly good at high frequencies, but not at low frequencies, when the bubbles are far apart. Note that the highest frequency used here, 30–31 bubbles per s, represents the limit at which the bubbles ($R_d - 0{\cdot}4$ cm) touch one another, and coalescence may be expected—at least near the injecting nozzle.

It is interesting that at low frequencies, up to 12–14 bubbles per s, the effect of bubble interaction is noted only through its effect on the temperature field. The tailing consecutive bubbles travel through the thermal field which was affected by the previous bubbles. Hence, the condensation rate decreases as compared with single bubble condensation, where the temperature driving force is unchanged along the bubbles path. However, at higher frequencies, as the bubbles enter the wake region of the preceding bubbles, the flow field is also affected and $U_\infty^F > U_\infty$. The increased convection enhances the transfer rate. Thus, these two factors—the increase in the field temperature and the rise velocity—adversely affect the condensation rate. Figures 7 and 8 with $F = 18$ represent an intermediate case, and as can be seen, the condensa-

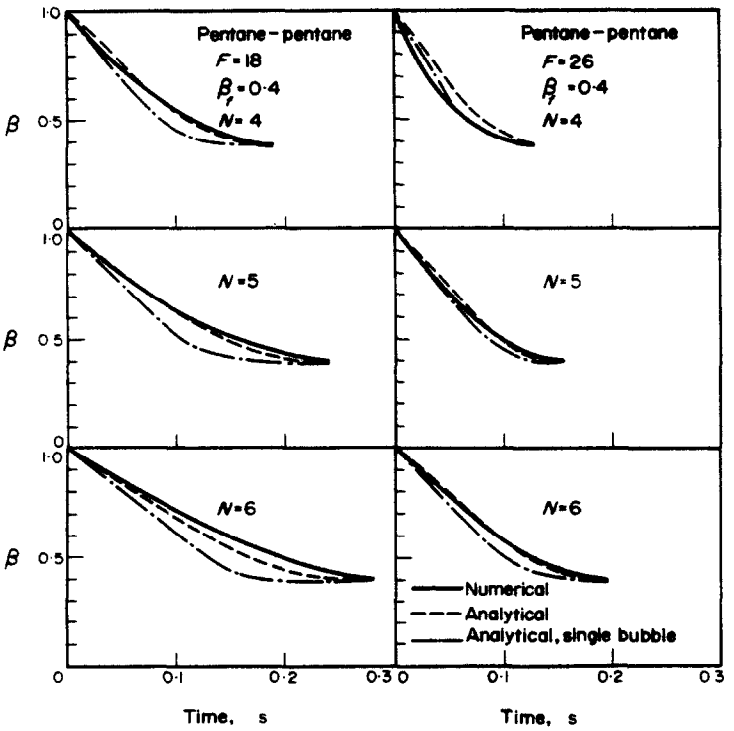

FIG. 7. Comparison of exact and approximate solutions, pentane–pentane system.

tion rate increases at higher frequencies ($F = 26$), approaching that of a single bubble. In general, the effect of frequency is more pronounced in the presence of inerts, since they affect only the temperature field and have but little effect on the rise velocity.

The satisfactory agreement between the exact and approximate "analytical" solution is highly rewarding in view of the complexity and technical difficulties associated with the exact numerical solution. It is important to note that the "exact" solution for a continuous bubble train is made possible by specifying a periodic steady state as well as a finite condensation time (= 99 per cent of maximum condensation possible at infinite time). The bubble row thus becomes finite, though the bubbles are replaced periodically, and the solution for the flow field becomes possible. The number of bubbles in a row, N, is defined by the relationship $t = (N - 1)/F$. Obviously, N is dependent on the actual operating conditions, namely ΔT^*, F and the inerts content (or β_f) and a solution is sought for conditions yielding integer number of bubbles in a row. (Note that at a constant F a low value of N is analogous to high ΔT^* and a large N represents a low ΔT^*.) In practice, however, the experimental data consists of ΔT^*, F and β_f (but not N!) and an exact solution based on this information, though possible, is tedious and time consuming. The "analytical" solution, on the other hand, does not require N to be *a priori* specified and one can therefore use it for comparison with the experimental data. The good agreement between the two theoretical solutions justified this time saving procedure.

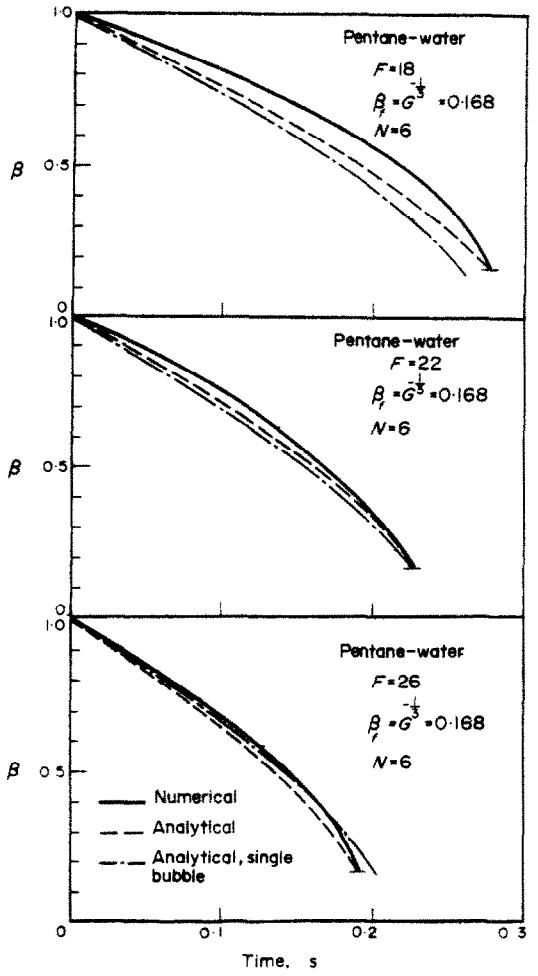

FIG. 8. Comparison of exact and approximate solutions, pentane–water system.

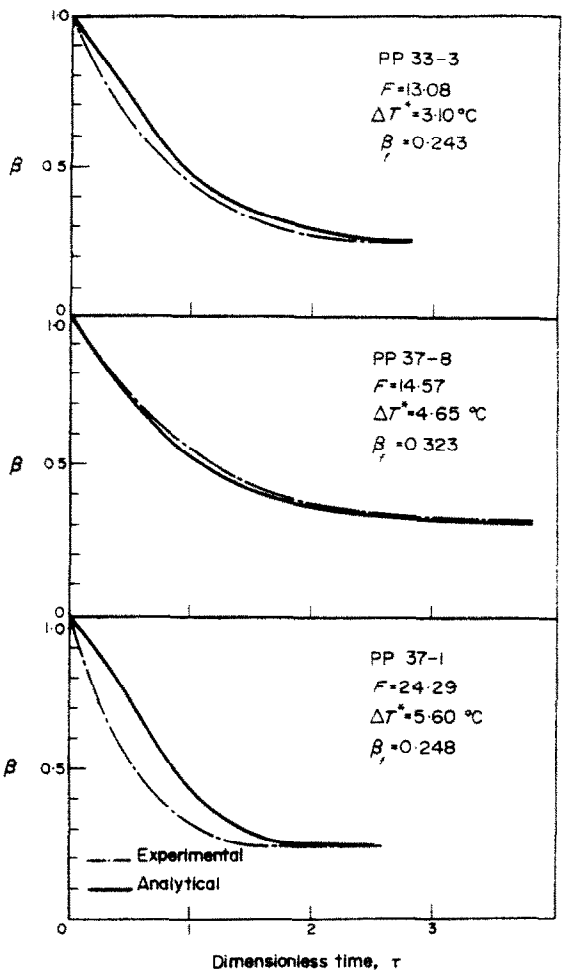

FIG. 9. Comparison of theoretical and experimental results, pentane–pentane system.

The pertinent dimensions of the bubbles, obtained by frame-by-frame analysis of the cine-camera films, were fed into a data reduction computer program which fits the data to exponential decay type curves. In the weighted non-linear least squares technique used, the residuals were weighted by calculated value based on the standard deviation of the measurements.

As seen from Figs. 9 and 10 the agreement between theory and experiment is generally quite good. However, at higher frequencies the theoretical values are rather conservative. This is undoubtedly due to deviation from the assumed axial-symmetry and larger (and possibly different) interaction effects—than accounted for—as the bubbles approach each other at higher frequencies. This is manifested by the noted increase in vibrations at the bubble's interface. Also to be noted is the difference between the theoretical and experimental curves at high inerts contents, particularly at the last condensation stages. This is due to the assumed homogeneous distribution of the non-

condensables within the bubble. As shown elsewhere [5] this can be corrected by considering a parabolic rather than an homogeneous distribution.

Finally, it is important to note that the relatively small effect of the frequency on the condensation rates, hence condensation height, of the bubbles in a bubble train is due to the fact that the (single) train is enclosed in an "infinite", heat absorbing, medium. However, in practice many adjacent trains are present and the temperature-increase along the column will be much more pronounced. Moreover, the rise velocity will also be affected, usually decreasing. Thus, pronounced effects of frequency on the collapse rate may be anticipated.

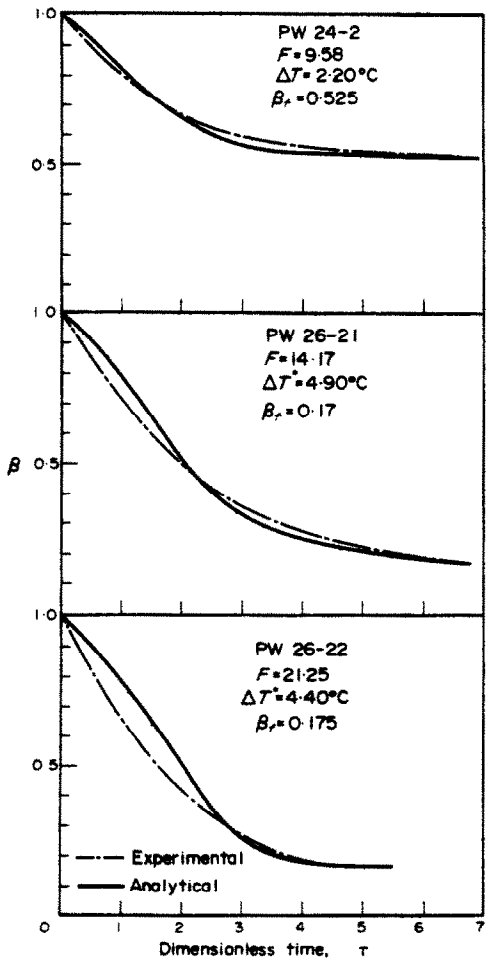

FIG. 10. Comparison of theoretical and experimental results, pentane–water system.

6. CONCLUSIONS

The condensation rate of a continuous bubble train rising from a single nozzle was solved by an iterative, simultaneous solution of the coupled flow and temperature fields. The reliability of the solution was demonstrated by its convergence to single-bubble condensation and by comparison with another solution [3] and with experimental data.

Frequency affects condensation rate by two counteracting effects: the temperature field and the rise velocity. The former is affected by the presence of non-condensables, while the latter, which becomes significant only at frequencies above 12–14 bubbles per s, is independent of inerts.

In general, at frequencies up to 20 bubbles per s, the collapse rate of a bubble train is smaller than that of a single bubble, and approaches the latter at high frequencies. However, the effect of frequency in multi-train systems is anticipated to be much larger, i.e. the collapse rate is much lower than that of a single bubble or even a (single) bubble train.[19].

REFERENCES

1. O. D. Wittke and B. T. Chao, Collapse of vapor bubbles with translatory motion, *J. Heat Transfer* **89**, 17 (1967).
2. S. Sideman and G. Hirsch, Direct contact heat transfer with change of phase; condensation of single vapor bubbles in an immiscible liquid medium, *A.I.Ch.E.Jl* **11**, 1019 (1965).
3. J. A. Isenberg and S. Sideman, Direct contact heat transfer with change of phase: bubble condensation in immiscible liquids, *Int. J. Heat Mass Transfer* **13**, 997 (1970).
4. J. Isenberg, D. Moalem and S. Sideman, Direct contact heat transfer with change of phase: bubble collapse with translatory motion in single and two-component systems, Heat Transfer Conference, Paris Vol. V, p. 258 (1970).
5. D. Moalem and S. Sideman, Bubble condensation with non-homogeneous distribution of non-condensables. *Int. J. Heat Mass Transfer* **14**, 2152 (1971).

6. D. MOALEM, S. SIDEMAN, A. ORELL and G. HETSRONI. Condensation of bubble train—an approximate solution, Proc. Int. Symp., Two-Phase Systems, Aug. 1971, Haifa, Israel, *Progress in Heat and Mass Transfer* Vol. 6, p. 155. Pergamon Press, Oxford (1972).
7. W. M. HICKS. On the motion of two spheres in a fluid, *Phil. Trans.* 455 (1880).
8. A. B. BASSET, On the motion of two spheres in a liquid, and allied problems, *Inc. Cond. Math. Soc.* **18**, 369 (1887).
9. P. MICHAEL, Ideal flow a long a row of spheres, *Physics Fluids* 8, 1263 (1965).
10. R. A. HERMAN, On the motion of two spheres in fluid, *Q. J. Mat.* **22**, 204 (1887).
11. J. ISENBERG and S. SIDEMAN, Flow field around collapsing bubble trains. Theoretical analysis, *Appl. Sci. Res.* **24**, 53 (1971).
12. T. ISHII and A. I. JOHNSON, Mass transfer without and with chemical reaction in dispersed gas–liquid two-phase flows, *Can. J. Chem. Engng* **48**, 56 (1970).
13. D. MOALEM, Single bubble and bubble train condensation in one and two component systems, D.Sc. Thesis (in Hebrew), Technion, Israel (1972).
14. W. L. HABERMAN and R. K. MORTON, An experimental study of bubbles moving in liquids, Navy Dept. Rept. No. 802, Washington, D.C. (1953); Am. Sci. Civil Eng. Paper 2799, p. 227 (1954).
15. L. B. TOROBIN and W. H. GAUVIN, Fundamental aspects of solid–gas flow, Part II. The sphere wake in steady laminar fluids, *Can. J. Chem. Engng* **37**, 167 (1959).
16. N. DE NEVERS and J. L. WU, Bubble coalescence in viscous fluids, *A.I.Ch.E.Jl* **18**, 182 (1971).
17. M. LINTON and K. L. SUTHERLAND, Transfer from a sphere into a fluid in laminar flow, *Chem. Engng Sci.* **12**, 214 (1960).
18. M. BENTWICH, G. SZWARCHAUM and S. SIDEMAN, Time dependent temperature distribution in flow past a sphere, Paper 65-HT-38, 8th National AIChE Heat Trans. Conf. (1965).
19. S. SIDEMAN and D. MOALEM, Direct contact heat exchangers: comparison of counter and co-current condensers, Proc. 4th Int. Symp. on Fresh Water From the Sea, Heidelberg, Vol. 1, p. 103 (Sept. 1973).

APPENDIX A

The Solution of the Temperature Field

In a finite difference form, using an implicit, backward difference technique, equation (21) becomes:

$$\bar{a}\theta_{i-1,j+1} + \bar{b}\theta_{i,j+1} + \bar{c}\theta_{i+1,j+1} = \bar{d} \qquad (A.1)$$

where

$$\bar{a} = \frac{A_t}{(\Delta\psi_t)^2} - \frac{B_t}{2\Delta\psi_t}; \qquad \bar{b} = \frac{c}{\Delta\phi} - \frac{2A_t}{(\Delta\psi_t)^2}$$

$$\bar{c} = \frac{A_t}{(\Delta\psi_t)^2} + \frac{B_t}{2\Delta\psi_t}; \qquad \bar{d} = \frac{C}{\Delta\phi}\cdot\theta_{i,j}.$$

Equation (A.1), subject to the boundary conditions, equation (23), is a diagonal matrix for each equipotential line. For the $j+1$ line this matrix is:

$$\begin{vmatrix} b_1 & c_1 & & & \\ a_2 & b_2 & c_2 & & \\ & a_3 & b_3 & c_3 \ldots & \\ & & & & \\ & & & a'_n & b_n \end{vmatrix} \begin{pmatrix} \theta_{1,j+1} \\ \theta_{2,j+1} \\ \vdots \\ \theta_{n,j+1} \end{pmatrix} = \begin{pmatrix} d'_1 \\ d_2 \\ \vdots \\ d_n \end{pmatrix} \qquad (A.2)$$

where

$$d'_1 = d_1 - a_1\theta_0; \qquad a'_n = a_n + c_n.$$

For a constant heat flux boundary conditions, i.e. the high frequency case, $c'_1 (= a_1 + c_1)$ replaces c_1 and $d'_1 = d_1$ in (A.2). The whole temperature field is solved by solving (A.2) successively for each of the equipotential lines.

Utilizing the geometrical relationship

$$\left.\frac{\partial T}{\partial n}\right|_{\psi_t=0} = \frac{\partial T}{\partial r}\cos(90-\gamma) - \frac{\partial T}{\partial z}\cos\gamma \qquad (A.3)$$

the local temperature gradient normal to the interface in the X–Y(or r–z) plane is given by:

$$\left.\frac{\partial T}{\partial n}\right|_{\psi_t=0} = -Y\frac{(T^* - T_\infty)}{D}\frac{\partial\theta}{\partial\psi_t}\left.\frac{(v_z\sin\gamma + v_r\cos\gamma)}{U^F_\infty}\right|_{\psi_t=0} \qquad (A.4)$$

where the dimensionless gradient along the $(j+1)$ equipotential line is approximated by the Lagrange 3-point formula, i.e.

$$\left.\frac{\partial\theta}{\partial\psi_t}\right|_{\psi_t=0} \approx \frac{1}{2(\Delta\psi_t)}(-3\theta_{0,j+1} + 4\theta_{1,j+1} - \theta_{2,j+1}). \qquad (A.5)$$

Finally, the collapse rate, equation (25), is calculated by

$$\dot{R} = \frac{k}{2\rho_{v,w}\lambda}\sum_{j=1}^{n}\frac{\overline{dT}}{dn}(\cos\gamma_j - \cos\gamma_{j+1}) \qquad (A.6)$$

where $\overline{dT}/dn$ is the average temperature gradient on the interface between points j and $j+1$, and where $j=1$ corresponds to the contact angle γ_c and $j=n$ corresponds to the separation angle γ_s.

APPENDIX B

Outline of Iteration Procedure

(a) Fix F;
(b) Fix N;
(c) Estimate R_i^0, using the approximate solution [6];
(d) Calc. U^F_∞ by equation (9) for the assumed row;
(e) Calc. the flow field (sec. 2.4);
(f) Assume ΔT^*, and solve for the temp. field (equation (21) and Appendix A) and collapse rate (equation A.6):

(g) Calc. R_i^{New}, equation (26), and establish new row;
(h) Repeat (d) to (f), if necessary, for ΔT^* so as to satisfy (b), till convergence of R_i;
(i) Change N and repeat (c) to (h);
(j) Change F and repeat (b) to (i).

TRANSFERT THERMIQUE DE CONTACT DIRECT AVEC CHANGEMENT DE PHASE: CONDENSATION D'UN TRAIN DE BULLES

Résumé—La résolution des champs couplés de vitesse et de température associés à la condensation d'un train de bulles à une ou deux phases est utilisée pour déterminer le rayon de la bulle en fonction du temps (ou de la hauteur), de la fréquence, de la température et de la concentration en composant inerte.

La validité de la procédure est démontrée par sa convergence à fréquence nulle avec les autres solutions de condensation d'une bulle unique et par le bon accord du calcul avec les données expérimentales.

WÄRMEÜBERTRAGUNG FÜR DIREKTEN KONTAKT BEI PHASENÄNDERUNG: DIE KONDENSATION EINER BLASENKETTE

Zusammenfassung—Die Lösung der gekoppelten Geschwindigkeits- und Temperaturfelder bei der Kondensation einer einphasigen oder zweiphasigen Blasenkette wird herangezogen, um die Radien der Blasen als eine Funktion der Zeit (oder Höhe), der Frequenz, des treibenden Temperaturgefälles und der Inertgaskonzentration zu erhalten.

Die Zuverlässigkeit des Lösungsweges wird gezeigt durch die Konvergenz bei der Frequenz Null gegenüber anderen Lösungen der Einzelblasenkondensation und durch die gute Übereinstimmung der berechneten Ergebnisse mit experimentellen Daten.

ПРЯМОЙ КОНТАКТНЫЙ ПЕРЕНОС ТЕПЛА ПРИ ФАЗОВОМ ПРЕВРАЩЕНИИ: КОНДЕНСАЦИЯ ЦЕПОЧКИ ПУЗЫРЕЙ

Аннотация—Решение взаимосвязанных полей скорости и температуры в случае конденсации одно- или двухфазной цепочки пузырей используется для нахождения радиуса пузырей в зависимости от времени (или высоты), частоты, температурного напора и концентрации инертных веществ.

Совпадение найденного решения с данными, полученными другими методами в случае конденсации отдельного пузыря, и с экспериментальными данными подтверждает надежность предложенного метода.